Analysis of the data base from a DNS of a separating turbulent boundary layer

By Martin Skote[*] and Dan S. Henningson[*†]

1. Motivation and objectives

This work was performed at CTR during a month-long visit in May 1999. The data base analyzed comes from a simulation performed by Na & Moin (1998*a*).

Although the data from the simulations have been used in the study of the structure of the wall pressure (Na & Moin 1998*b*), an analysis of the mean flow had not been conducted to a great extent. The aim of this work is to investigate the near wall scalings of the turbulent mean flow close to separation.

The scalings are very important for the correct behavior of wall damping functions used in turbulence models. For a zero pressure gradient (ZPG) boundary layer, the damping functions and boundary conditions in the logarithmic layer are based on a theory where the friction velocity,

$$u_\tau \equiv \sqrt{\nu \left.\frac{\partial u}{\partial y}\right|_{y=0}}, \tag{1}$$

is used as a velocity scale. However, in the case of a boundary layer under an adverse pressure gradient (APG), u_τ is not the correct velocity scale, especially not for a strong APG and low Reynolds number. In the case of separation this is clear since u_τ becomes zero. In a number of studies the case of separation has been investigated. The various theories will be presented in the section where the analysis is presented.

Also, for moderate pressure gradients, the near wall region is influenced if the Reynolds number is low enough. The combination of a pressure gradient and low Reynolds number give a flow that deviates from the classical near wall laws. The equations governing the inner part of the boundary layer can be analyzed, and the theory is applicable to the results from the direct numerical simulations investigated here.

In section 2 the numerical method and flow geometry is briefly described. The results from the investigation of the mean flow are presented in four parts in section 3. The first part (3.1) is devoted to the total shear stress. Here

[*]Department of Mechanics, Royal Institute of Technology (KTH), SE-100 44 Stockholm, Sweden
[†]Aeronautical Research Institute of Sweden (FFA), Box 11021, SE-161 11 Bromma, Sweden

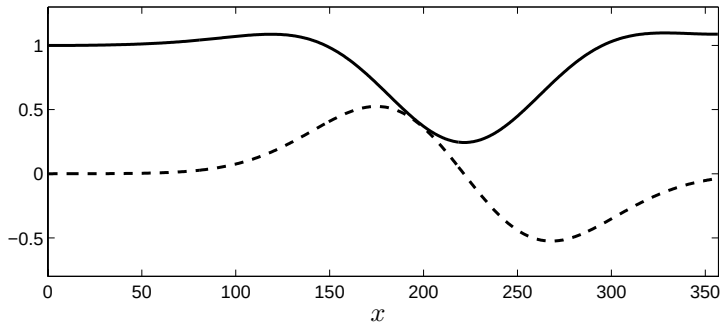

FIGURE 1. Freestream velocity. — : U; - - : V.

the alternative velocity scale based on the pressure gradient is introduced, and the effect of the APG on the inner part of the boundary layer is discussed. Continued investigation of the total shear stress in the second part (3.2) leads to the logarithmic law of the velocity profile. The law is extended to the APG case and is shown to be in fair agreement with DNS data. To further investigate the different velocity scales, the viscous sub-layer is investigated in the third part (3.3). And finally, in the fourth part (3.4), some earlier theories regarding the APG flow and separation are briefly presented.

2. Numerical method and flow characteristics

The simulation evaluated here was performed by Na & Moin (1998*a*), using a second-order finite difference method. The computational box was $350\times64\times50$ based on the δ^* at the turbulent inflow. The number of modes was $513\times193\times129$. The inflow condition was taken from Spalart's ZPG simulation. It consists of a mean turbulent velocity profile with superimposed turbulence with randomized amplitude factors while the phase was unchanged. The boundary conditions applied on the upper boundary are the prescribed wall normal velocity and zero spanwise vorticity,

$$v(x, L_y, z) = V(x) \qquad \left.\frac{\partial u}{\partial y}\right|_{x,L_y,z} = \frac{dV(x)}{dx}. \tag{2}$$

In Fig. 1 the two components of the freestream velocity are shown as a function of the downstream coordinate x. The two components are denoted U and V in the streamwise and wall normal directions respectively. Elsewhere in the flow the two components of the mean velocity are denoted u and v. There is no third direction in the mean flow.

The wall normal velocity (V) is prescribed in order to create a separation bubble. The point of separation is at $x = 158$, and the reattachment occurs at $x = 257$.

V varies in the downstream direction and thus induces a gradient in the u component at the freestream boundary, due to the zero vorticity condition.

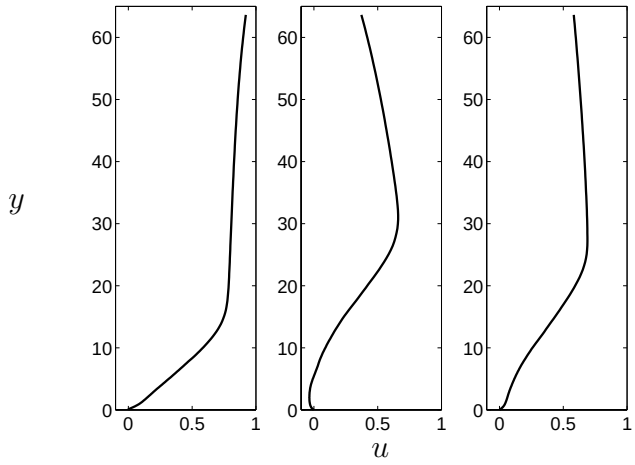

FIGURE 2. Velocity profiles at $x = 157$, 200, and 260.

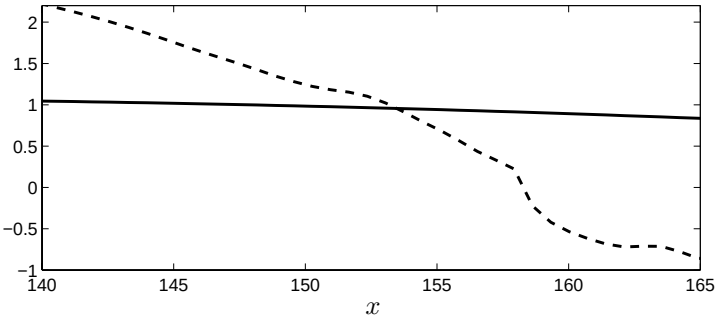

FIGURE 3. In the vicinity of the separation. — : U; - - : $u_\tau \times 100$.

In Fig. 2 three velocity profiles are shown from different downstream positions before, inside, and after the separation bubble. The gradients at the freestream boundary due to the boundary conditions are clearly visible. Since the boundary conditions applied in the simulation do not allow the $y-$derivative of the velocity profile to be zero at the upper boundary, all quantities involving δ^* or other integral quantities become ambiguous. The near wall behavior is not influenced by this gradient, and the analysis of the boundary layer equations can be compared with the DNS data.

The quantities shown in Fig. 3 as a function of the downstream direction in the vicinity of the separation are U and u_τ. There is a strong variation of u_τ at the point of separation as seen in Fig. 3.

3. Mean flow profiles

In this section the existing theoretical theories will be presented together with results from the DNS. Much of the theory is based on the two distinct regions

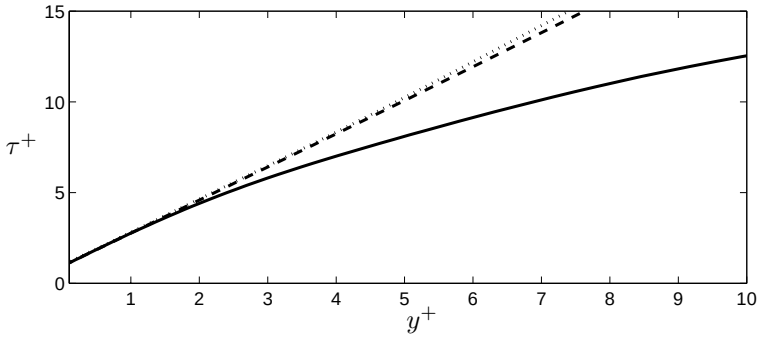

FIGURE 4. Total shear stress at $x = 150$. — : DNS; - - : Eq. (4); $\cdots$: Eq. (5).

of the flow, the inner and outer part respectively. Since only the inner part of the boundary layer will be considered here, the theory concerning the outer part is omitted.

3.1. *The total shear stress*

When neglecting the non-linear, advective terms in the equations describing the mean flow, the equation governing the inner part of the boundary layer is obtained. This equation can, when using the inner length and velocity scales ν/u_τ and u_τ be written,

$$0 = -\frac{\nu}{u_\tau^3}\frac{1}{\rho}\frac{dP}{dx} + \frac{d^2u^+}{dy^{+2}} - \frac{d}{dy^+}\langle u'v'\rangle^+, \tag{3}$$

where $\langle u'v'\rangle$ is the Reynolds shear stress. If the term involving the pressure gradient is smaller than the other terms, the equation reduces to the equation governing the inner part of a ZPG boundary layer. However, for the APG case considered here, this term cannot be neglected. Equation (3) can be integrated to give an expression for the total shear stress,

$$\tau^+ \equiv \frac{du^+}{dy^+} - \langle u'v'\rangle^+ = 1 + \frac{\nu}{u_\tau^3}\frac{1}{\rho}\frac{dP}{dx}y^+ \tag{4}$$

The total shear stress, τ^+, from the DNS and the curve $\tau^+(y^+)$ represented by Eq. (4) are shown in Fig. 4 at the position $x = 150$. The third and dotted line is obtained when considering that the pressure gradient is slightly dependent on the wall normal coordinate, in which case the integration of Eq. (3) yields,

$$\tau^+ = 1 + \int_0^{y^+} \frac{\nu}{u_\tau^3}\frac{1}{\rho}\frac{dP}{dx}(y^+)dy^+. \tag{5}$$

As seen in Fig. 4, the two expressions (4) and (5) are nearly identical. For a zero pressure gradient case, Eq. (4) predicts a constant shear stress of unity.

The pressure gradient term in Eq. (4) is evidently important for the shear stress distribution in the inner part of the boundary layer. This was observed in,

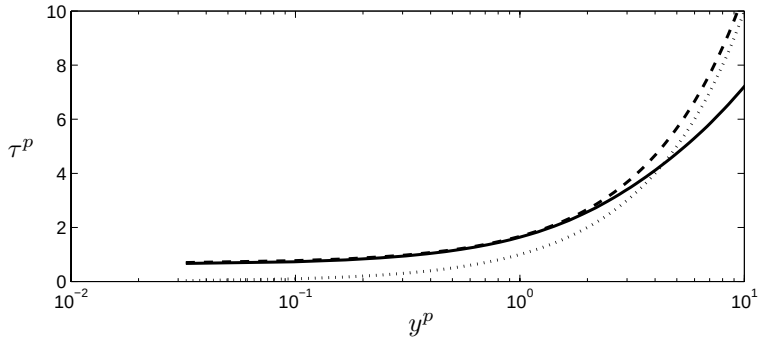

FIGURE 5. Total shear stress at $x = 150$. — : DNS; - - : Eq. (8); $\cdots$: asymptotic profile $\tau^p = y^p$.

among others, the experiments by Bradshaw (1967), Samuel & Joubert (1974) and Skåre & Krogstad (1994). It can be shown that the pressure gradient term decreases with increasing Reynolds number. The term is thus important only for low Reynolds numbers. However, close to separation, where u_τ approaches zero, it is clear that the terms becomes infinite even for large Reynolds numbers.

When considering separation the singularity mentioned above can be avoided by introducing the velocity scale,

$$u_p \equiv \left(\nu \frac{1}{\rho} \frac{dP}{dx}\right)^{1/3}. \tag{6}$$

First Eq. (4) is formulated as

$$\tau^+ = 1 + (\frac{u_p}{u_\tau})^3 y^+. \tag{7}$$

The velocity scale u_p has to be used instead of u_τ if the last term in Eq. (7) becomes very large, which happens if $u_\tau \ll u_p$, i.e. the boundary layer is close to separation. This was noted by Stratford (1959), Townsend (1961) and Tennekes & Lumley (1972). By multiplying Eq. (7) by $(u_p/u_\tau)^2$, the following expression for $\tau^p \equiv \tau/u_p^2$ is obtained,

$$\tau^p = y^p + (\frac{u_\tau}{u_p})^2, \tag{8}$$

with the asymptotic form $\tau^p = y^p$ when separation is approached, where $y^p \equiv yu_p/\nu$. Thus, in this rescaled form, the singularity is avoided.

In Figs. 5 and 6 the shear stress scaled with u_p is shown at $x = 150$ and $x = 158$. Both the linear expression (8) and its asymptotic form are shown. At $x = 150$ the separation has not been reached, thus the asymptotic version deviates while the profile from Eq. (8) coincides with the DNS data. At $x = 158$ the asymptotic expression agrees with the profile from DNS since $u_\tau = 0$ at that position.

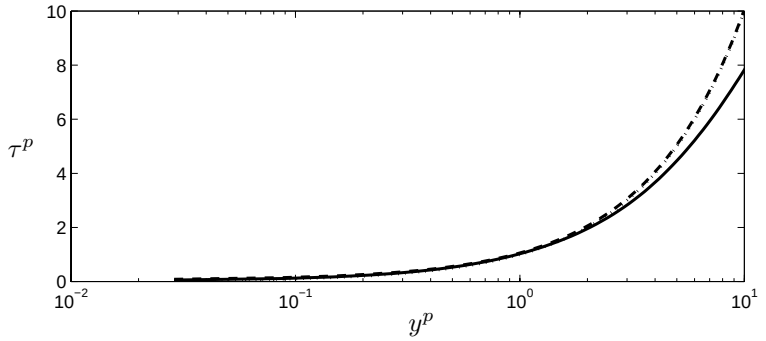

FIGURE 6. Total shear stress at $x = 158$. — : DNS; - - : Eq. (8); $\cdots$: asymptotic profile $\tau^p = y^p$.

3.2. *The logarithmic region*

Now, when the velocity scale u_p has been introduced, it is possible to investigate how other theoretical results for a ZPG turbulent boundary layer can be modified by the presence of an APG.

The Eq. (3) and the equation for the outer part of the boundary layer constitute a problem with inner and outer solutions. This problem has been treated with the method of matched asymptotic expansions by, among others, Mellor (1972) and Afzal (1996). The aim is to obtain higher order terms in the matching of the inner and outer solutions. The small parameter that is used in the expansions is u_τ/U, which is related to the Reynolds number through the logarithmic friction law.

The presentation here will be very brief and only the inner part is discussed. For the ZPG case, the scaling of the total shear stress with u_τ gives a self-similar profile ($\tau^+ = 1$). From Eqs. (7) and (8) it is observed that neither u_τ nor u_p as velocity scale results in a self-similar expression. However, Eq. (4) can be formulated as

$$\tau^* \equiv \frac{1}{u_*^2}\left(\nu\frac{\partial u}{\partial y} - \langle u'v'\rangle\right) = 1, \tag{9}$$

where u_* is a velocity scale that depends on y and can be expressed in either plus or pressure gradient units,

$$u_*^2 = u_\tau^2 + \frac{u_p^3}{u_\tau}y^+ = u_\tau^2 + u_p^2 y^p. \tag{10}$$

Thus, by scaling the total shear stress with u_*, a self-similar expression is obtained ($\tau^* = 1$).

For the ZPG case, the matching of the inner and outer equations results in the equation,

$$y^+\frac{du^+}{dy^+} = \frac{1}{\kappa}. \tag{11}$$

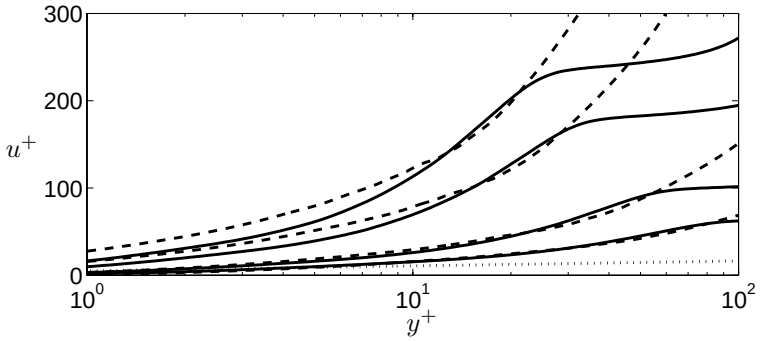

FIGURE 7. Velocity profiles. — : DNS; - - : Eq. (15) with $\kappa = 0.41$ and $B = -2$; $\cdots$: $u^+ = \frac{1}{0.41} \ln y^+ + 5.1$.

If now u_* is used as the velocity scale, the velocity gradient can be formulated as,

$$\nu \frac{\partial u}{\partial y} \frac{1}{u_*^2} = \left(\frac{\partial u}{\partial y} \right)^* . \tag{12}$$

The matching between the inner and outer equations as described by Afzal (1996) results in

$$y^* \left(\frac{\partial u}{\partial y} \right)^* = \frac{1}{\kappa}, \tag{13}$$

where

$$y^* \equiv y u_* / \nu = \sqrt{(y^+)^2 + (y^p)^3}. \tag{14}$$

In the same way as Eq. (11) can be integrated to give the logarithmic law for the ZPG case, Eq. (13) above can be integrated. However, Eq. (13) must be formulated with either u_τ or u_p as velocity scale before being integrated. If u_τ is chosen as velocity scale, the integration of Eq. (13) yields,

$$u^+ = \frac{1}{\kappa} \left(\ln y^+ - 2 \ln \frac{\sqrt{1 + \lambda y^+} + 1}{2} + 2(\sqrt{1 + \lambda y^+} - 1) \right) + B, \tag{15}$$

with

$$\lambda = \left(\frac{u_p}{u_\tau} \right)^3 . \tag{16}$$

The expression (15) is not self-similar due to the term λ, which is Reynolds number dependent.

Equation (15) is the same expression as Afzal (1996) arrived at. It is also similar to the equation which Townsend (1961) derived from mixing length arguments. The velocity profiles from the DNS of Na and Moin close to the point of separation are shown together with the standard log-law and the extended log-law (15) in Fig. 7. The separation occurs at $x = 158$ and the four velocity profiles are shown at $x = 150, 155, 157, 158$.

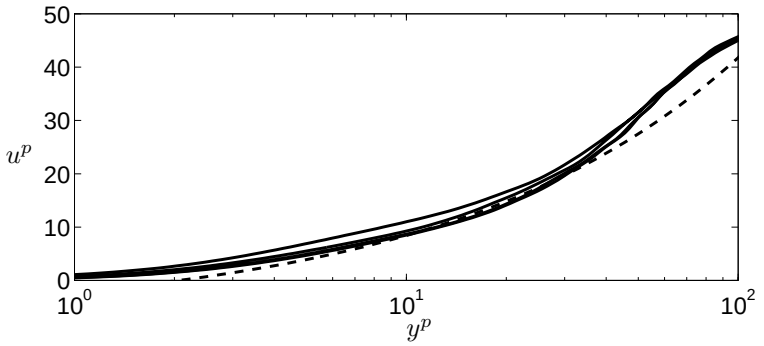

FIGURE 8. Velocity profiles. — : DNS; - - : Eq. (18) with $\kappa = 0.41$ and $C = -7$.

From Fig. 7 it is clear that the logarithmic law, valid for ZPG flows, is a poor instrument for obtaining boundary conditions in the log-layer for turbulence models. The extended log-layer, which involves the pressure gradient, seems to capture the deviation from the logarithmic profile surprisingly well. The parameters κ and B have not been adjusted to fit the DNS data; rather, the standard values have been used. In addition, the region where Eq. (15) is valid can be discussed.

When $u_p \to 0$, Eq. (13) reduces to the equivalent equation for the ZPG case (11), and the usual log-law is recovered. If $u_\tau \to 0$, Eq. (13) reduces to,

$$\sqrt{y^p}\frac{\partial u^p}{\partial y^p} = \frac{1}{\kappa}, \tag{17}$$

and the half-power law is obtained,

$$u^p \equiv \frac{u}{u_p} = \frac{1}{\kappa} 2\sqrt{y^p} + C, \tag{18}$$

which was first obtained by Stratford (1959).

Since it is shown that the scaling based on u_p is preferred over u_τ close to separation, the profiles in Fig. 7 should collapse better when scaled with u_p. The same velocity profiles as in Fig. 7 are plotted together with the half-power law (18) in Fig. 8.

An interesting observation is that Eq. (18) leads to a shape factor of two with a small correction due to the constant C. The correction vanishes for large Reynolds numbers when $u_p/U \to 0$. In both DNS at low Reynolds numbers (Spalart & Leonard 1987) and experiments at large Reynolds numbers (Skåre & Krogstad 1994) of flows near separation, a shape factor close to two was observed. The shape factor is 1.8 at separation for the flow of Na and Moin. But, as discussed earlier, the gradient of the velocity profile at the upper boundary give a value of the shape factor that cannot be considered a proper one.

By expressing Eq. (13) in pressure gradient units and integrating, the following expression for u^p is obtained,

$$u^p = \frac{1}{\kappa}\left(2\sqrt{\gamma^2 + y^p} + \gamma \ln y^p - 2\gamma \ln(\sqrt{\gamma^2 + y^p} + \gamma)\right) + C, \tag{19}$$

where

$$\gamma = \frac{u_\tau}{u_p}.$$

In the limit of $u_\tau \to 0$, Eq. (18) is recovered. The velocity profiles collapse much better in the pressure gradient scaling as can be seen from Fig. 8 where the asymptotic profile (18) is also shown. The profiles obtained from Eq. (19) do not vary much for different downstream positions, hence only the asymptotic profile is shown.

The two expressions (15) and (19) are equivalent; only the choice of scaling when integrating Eq. (13) differs. They are both dependent on the Reynolds number through the terms λ and γ respectively. Equation (13) cannot be integrated directly to yield $u^*(y^*)$ independent on the Reynolds number. This is due to the term

$$\left(\frac{\partial u}{\partial y}\right)^*,$$

which cannot be expressed in only $u^* \equiv u/u_*$ and y^*. However, these arguments regarding the lack of self-similarity of the velocity profile will be clearer if the viscous sub-layer, where the Reynolds stress can be neglected, is considered.

3.3. *The viscous sub-layer*

In the viscous sub-layer the Reynolds shear stress approaches zero and Eq. (8) can be integrated to give,

$$u^p = \frac{1}{2}y^{p2} + \left(\frac{u_\tau}{u_p}\right)^2 y^p \tag{20}$$

In plus units this equation becomes,

$$u^+ = y^+ + \frac{1}{2}\left(\frac{u_p}{u_\tau}\right)^3 y^{+2}. \tag{21}$$

This equation reduces to the usual linear profile in ZPG case.

Figure 9 shows velocity profiles near the wall for $x = 150$ and $x = 158$ in plus units. The higher profile is located at $x = 158$. The solid lines are DNS data and the dashed ones are the profiles from Eq. (21). The dotted line is the profile valid for the ZPG case ($u_p = 0$). As seen from Fig. 9, the linear approximation works reasonably well at $x = 150$, upstream of separation. But at $x = 158$, the effect from the pressure gradient is too large. The profiles diverge as separation is approached since the second term in Eq. (21) becomes infinite.

Figure 10 shows velocity profiles near the wall for $x = 150$ and $x = 158$ in pressure gradient units. The higher profile is located at $x = 150$. In this

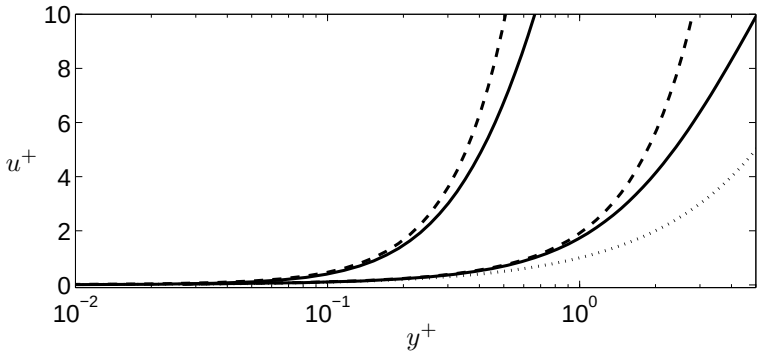

FIGURE 9. Velocity profiles at $x = 150$ and $x = 158$. — : DNS; - - : $y^+ + \frac{1}{2}\left(\frac{u_p}{u_\tau}\right)^3 y^{+2}$; $\cdots$: y^+.

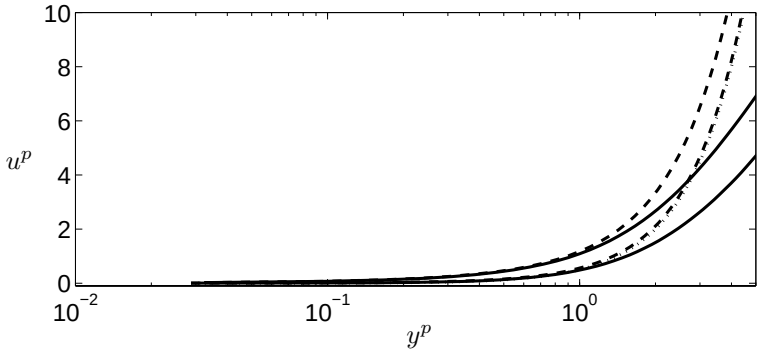

FIGURE 10. Velocity profiles at $x = 150$ and $x = 158$. — : DNS; - - : $\frac{1}{2}y^{p2} + (\frac{u_\tau}{u_p})^2 y^p$; $\cdots$: $\frac{1}{2}y^{p2}$.

case the asymptotic profile (dotted) is valid at separation. The solid lines are DNS data and the dashed are the profiles given by Eq. (20). From Fig. 10 one can draw the conclusion that the pressure gradient scaling is preferred since the profiles approach an asymptotic profile instead of diverging infinitely as u_τ approaches zero.

In both the viscous and logarithmic region, the velocity has been scaled with two different velocities, u_τ and u_p. Both of these scalings give in an asymptotic state a Reynolds number independent expression. The representations in plus units, Eqs. (15) and (21), return to the ZPG formulation when u_p approaches zero. The representation in pressure gradient units, Eqs. (19) and (20), become the square-root and square profiles when separation is approached.

In both these scalings the velocity profile is dependent of the ratio between u_τ and u_p as seen in the four equations mentioned above. However, the total

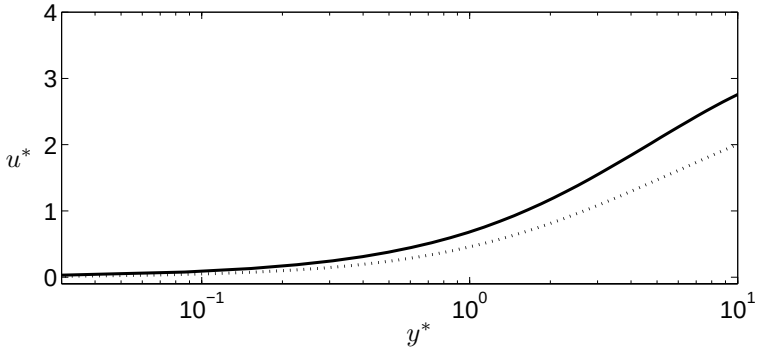

FIGURE 11. Velocity profiles at $x = 150$ and $x = 158$. — : DNS at $x = 150$; $\cdots$: DNS at $x = 158$.

shear stress could be made independent of this ratio by scaling with u_*, Eq. (9). Thus the profiles are self-similar with respect to Reynolds number and pressure gradient. In order to obtain an expression for the velocity scaled with u_* in the viscous sub-layer, Eq. (9) with the Reynolds stress equal to zero must be solved. Thus, it is

$$\nu \frac{\partial u}{\partial y} \frac{1}{u_*^2} = 1. \tag{22}$$

that needs to be solved. The solution $u^*(y^*)$ should be independent of the ratio between u_τ and u_p. Equation (22) formulated in star units gives

$$\frac{\partial u^*}{\partial y^*} + \frac{1}{2} \left(\frac{y^p}{y^*} \right)^3 \left(y^* \frac{\partial u^*}{\partial y^*} + u^* \right) = 1, \tag{23}$$

where the relation between y^* and y^p is given by Eq. (14), which can be written

$$y^{*2} = \left(\frac{u_\tau}{u_p} \right)^2 (y^p)^2 + (y^p)^3. \tag{24}$$

The ratio between u_τ and u_p is still present in Eq. (24), thus no independent solution can be found. This is also evident from DNS data where the profiles are scattered for different downstream positions as shown in Fig. 11.

3.4. *Comparison with other theories for the logarithmic region*

According to Tennekes & Lumley (1972), the scaling with pressure gradient velocity u_p should lead to the same form of matching as in the zero pressure gradient case. From this assumption a logarithmic law is obtained in the same manner as the usual procedure of matching the outer and inner solutions. The log-law becomes,

$$u^p = \frac{1}{\kappa} \ln(y^p) + B. \tag{25}$$

Equation (25) is shown in Fig. 12 together with DNS data from the positions $x = 150$ and $x = 158$.

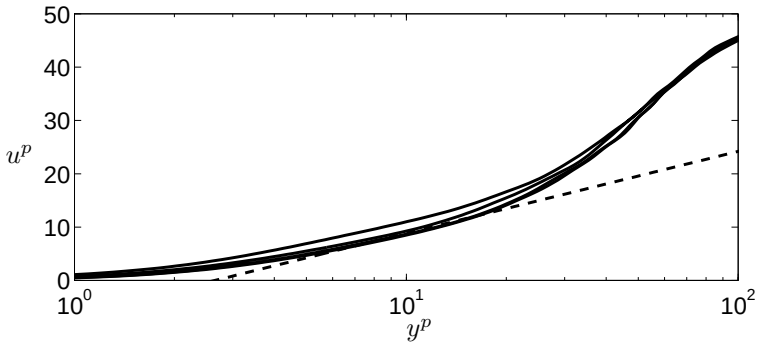

FIGURE 12. Velocity profiles. — : DNS; - - : Eq. (25) with $\kappa = 0.15$, $B = -6.5$.

According to Stratford (1959), the velocity profile should be a half-power law close to separation. Also Yaglom (1979) showed that a dimensional analysis gives the following expression for the velocity profile close to separation,

$$u^+ = K^+\sqrt{\lambda y^+} + K_1^+, \tag{26}$$

which can be expressed in pressure gradient scaling,

$$u^p = K\sqrt{y^p} + K_1. \tag{27}$$

Yaglom (1979) also proposed a fairly complicated dependence of K and K_1 on u_p and u_τ. This dependency was introduced to extend the theory valid at separation to the region upstream of detachment. It cannot be regarded as a sound procedure to incorporate a functional behavior in constants of an expression valid only in an asymptotic state. It seems to be a better approach to the equations to introduce the mixed velocity scale u_* and do the analysis leading to Eq. (19).

4. Conclusion

The scalings in the near wall region of a turbulent boundary layer close to separation have been analyzed. Two different velocity scales appears naturally in the governing equation: the friction velocity and the pressure gradient velocity. With the aid of the momentum equation governing the inner part, it is possible to derive a mixed velocity scale. By using this velocity scale and matching the inner and outer solutions, an extended logarithmic law is obtained. When approaching the zero pressure gradient case, the familiar log-law and plus scales are recovered. In the limit of separation, the half-power law in pressure gradient scaling is obtained. In the vicinity of separation, the extended logarithmic law in plus scaling give profiles in agreement with DNS data. The profiles are widely scattered when using the friction velocity as a velocity scale due to the large variation of the friction velocity in the vicinity of separation. When using pressure gradient scalings, the profiles are much less scattered, and the

extended logarithmic law in its asymptotic form (half-power law) agrees with the DNS data.

The mixed velocity scale, which depends on y, was shown to give self-similar profiles for the total shear stress. For the velocity however, no such profiles can be derived. Thus, for practical purposes such as boundary conditions for RANS-modeling and wall-damping functions, the extended logarithmic law should give more reasonable results than the corresponding zero pressure gradient laws. When the friction velocity varies rapidly or approaches zero, the scaling with pressure gradient velocity is preferred since the singularity at separation is avoided.

Even in the viscous sub-layer, the pressure gradient influences the velocity profile if the Reynolds number is low enough. The two velocity scales based on the friction velocity and pressure gradient velocity give profiles that are independent on Reynolds number only in the limit of zero pressure gradient and separation respectively. The comparison with data in the viscous sub-layer from direct numerical simulation shows that the velocity scale based on the pressure gradient can indeed be used in this region of the flow close to separation. In fact, such scaling shows that the velocity profiles approach an asymptotic, self-similar profile at separation. If the friction velocity scaling is used, the profiles diverge as separation is approached. This scaling gives an asymptotic self-similar profile (the linear profile) in the limit of zero pressure gradient.

References

Afzal, N. 1996 Wake layer in a turbulent boundary layer with pressure gradient: a new approach. In *IUTAM Symposium on Asymptotic Methods for Turbulent Shear flows at High Reynolds Numbers* (ed. K. Gersten), pp. 95–118. Kluwer Academic Publishers.

Bradshaw, P. 1967 The turbulent structure of equilibrium boundary layers. *J. Fluid Mech.* **29**, 625–645.

Mellor, G. L. 1972 The large reynolds number, asymptotic theory of turbulent boundary layers. *Intl J. Engng Sci.* **10**, 851–873.

Na, Y. & Moin, P. 1998*a* Direct numerical simulation of a separated turbulent boundary layer. *J. Fluid Mech.* **374**, 379–405.

Na, Y. & Moin, P. 1998*b* The structure of wall-pressure fluctuations in turbulent boundary layers with adverse pressure gradient and separation. *J. Fluid Mech.* **377**, 347–373.

Samuel, A. E. & Joubert, P. N. 1974 A boundary layer developing in an increasingly adverse pressure gradient. *J. Fluid Mech.* **66**, 481–505.

Skåre, P. E. & Krogstad, P.-Å. 1994 A turbulent equilibrium boundary layer near separation. *J. Fluid Mech.* **272**, 319–348.

Spalart, P. R. & Leonard, A. 1987 Direct numerical simulation of equilibrium turbulent boundary layers. In *Turbulent Shear Flows 5* (eds. F. Durst, B. E.

Launder, J. L. Lumley, F. W. Schmitd & J. H. Whitelaw), pp. 234–252. Springer-Verlag.

Stratford, B. S. 1959 The prediction of separation of the turbulent boundary layer. *J. Fluid Mech.* **5**, 1–16.

Tennekes, H. & Lumley, J. L. 1972 *A First Course in Turbulence*. The MIT Press.

Townsend, A. A. 1961 Equilibrium layers and wall turbulence. *J. Fluid Mech.* **11**, 97–120.

Yaglom, A. M. 1979 Similarity laws for constant-pressure and pressure-gradient turbulent wall flows. *Ann. Rev. Fluid Mech.* **11**, 505–40.